

Radiative Decays of the Higgs Boson to a Pair of Fermions

Tao Han^{a,b} and Xing Wang^a

^a*Pittsburgh Particle physics, Astrophysics, and Cosmology Center,
Department of Physics and Astronomy, University of Pittsburgh,
3941 O'Hara St., Pittsburgh, PA 15260, USA*

^b*Department of Physics, Tsinghua University, and Collaborative Innovation Center of Quantum
Matter, Beijing, 100086, China*

E-mail: than@pitt.edu, xiw77@pitt.edu

ABSTRACT: We revisit the radiative decays of the Higgs boson to a fermion pair $h \rightarrow f\bar{f}\gamma$ where f denotes a fermion in the Standard Model (SM). We include the chirality-flipping diagrams via the Yukawa couplings at the order $\mathcal{O}(y_f^2\alpha)$, the chirality-conserving contributions via the top-quark loops of the order $\mathcal{O}(y_t^2\alpha^3)$, and the electroweak loops at the order $\mathcal{O}(\alpha^4)$. The QED correction is about $Q_f^2 \times \mathcal{O}(1\%)$ and contributes to the running of fermion masses at a similar level, which should be taken into account for future precision Higgs physics. The chirality-conserving electroweak-loop processes are interesting from the observational point of view. First, the branching fraction of the radiative decay $h \rightarrow \mu^+\mu^-\gamma$ is about a half of that of $h \rightarrow \mu^+\mu^-$, and that of $h \rightarrow e^+e^-\gamma$ is more than four orders of magnitude larger than that of $h \rightarrow e^+e^-$, both of which reach about 10^{-4} . The branching fraction of $h \rightarrow \tau^+\tau^-\gamma$ is of the order 10^{-3} . All the leptonic radiative decays are potentially observable at the LHC Run 2 or the HL-LHC. The kinematic distributions for the photon energy or the fermion pair invariant mass provide non-ambiguous discrimination for the underlying mechanisms of the Higgs radiative decay. We also study the process $h \rightarrow c\bar{c}\gamma$ and evaluate the observability at the LHC. We find it comparable to the other related studies and better than the $h \rightarrow J/\psi \gamma$ channel in constraining the charm-Yukawa coupling.

Contents

1	Introduction	1
2	$h \rightarrow f\bar{f}(\gamma)$ at One-Loop	3
2.1	$\mathcal{O}(y_f^2\alpha)$ corrections	3
2.2	$\mathcal{O}(y_t^2\alpha^3, \alpha^4)$ corrections	4
2.3	Partial decay widths	5
3	LHC Search for $\ell^+\ell^-\gamma$	8
3.1	$h \rightarrow \gamma^*\gamma \rightarrow \ell^+\ell^-\gamma$	9
3.2	$h \rightarrow Z\gamma \rightarrow \ell^+\ell^-\gamma$	11
3.3	$h \rightarrow J/\psi \gamma \rightarrow \ell^+\ell^-\gamma$	12
3.4	$h \rightarrow \tau^+\tau^-\gamma$	13
4	LHC Search for $c\bar{c}\gamma$ and the Charm-Yukawa Coupling	13
5	Summary	16

1 Introduction

The discovery of the Higgs boson at the CERN Large Hadron Collider (LHC) has set a milestone in particle physics. All the studies indicate that it is consistent with the Standard Model (SM) Higgs boson. However, there are only a handful channels observed at the LHC and accuracies on the branching fraction measurements, even assuming it is the SM Higgs boson, are still no better than about 10%. There are compelling motivations that the SM needs to be extended, including the particle dark matter, the origin of the neutrino mass, and perhaps the most puzzling related to the electroweak scale, the “naturalness” for the Higgs boson mass in the SM. Therefore, more detailed studies regarding the properties of the Higgs boson are necessary to test the SM and to look for possible new physics beyond the Standard Model.

With a large amount of data being accumulated at the LHC Run-2 and the higher luminosity expectation of 3 ab^{-1} (HL-LHC), one would expect to produce a large sample, eventually reaching about $50 \text{ pb} \times 3 \text{ ab}^{-1} \approx 150$ million Higgs bosons. As thus, searching for rare decays of the Higgs boson becomes feasible and thus increasingly important to test the Higgs sector in the Standard Model and to seek for new physics beyond the SM. One important feature of the Higgs boson predicted by the SM is that the Higgs-fermion interaction strength, the Yukawa coupling, is proportional to the fermion mass. So far, ATLAS [1–3] and CMS [4–6] have only been able to measure the Higgs couplings to the third-generation fermions (τ and b directly and t indirectly). The Higgs rare decays to a

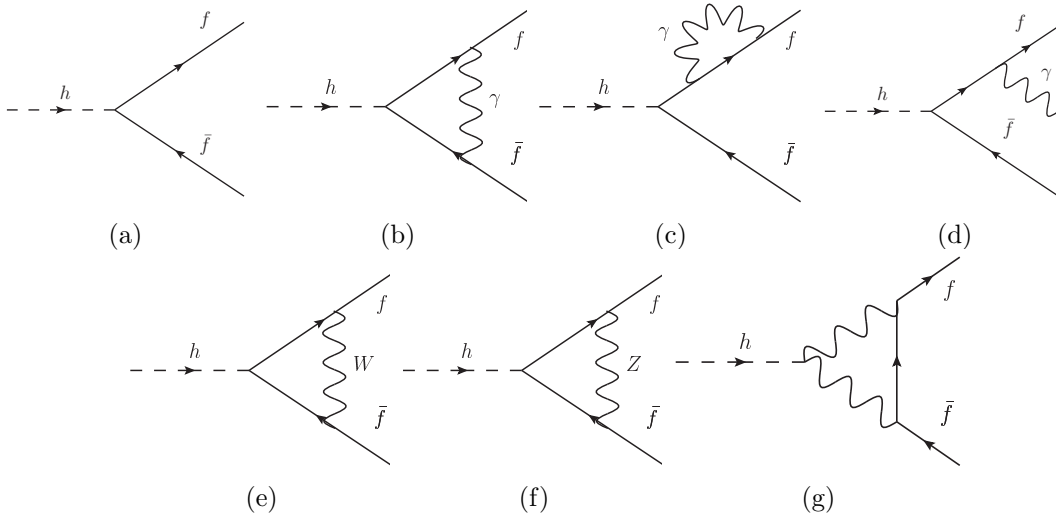


Figure 1: Representative Feynman diagrams of $h \rightarrow f\bar{f}$ and its EW radiative corrections up to $\mathcal{O}(y_f^2\alpha)$.

light fermion pair are usually very difficult to observe because of the suppression by the small Yukawa couplings. For instance, the branching fraction of $h \rightarrow e^+e^-$ is $\mathcal{O}(10^{-8})$, and thus hopeless to detect this decay channel at colliders. In this paper, we study other rare decay channels: the Higgs radiative decay to a fermion pair $h \rightarrow f\bar{f}\gamma$. Firstly, this decay channel receives contribution that is proportional to the Higgs-fermion interaction strength, which may provide a complementary way to measure certain Yukawa couplings. Secondly, as it also receives contributions from electroweak (EW) one-loop diagrams [7], this channel is not necessarily governed by the Yukawa coupling for light fermions, leading to violation of the Yukawa scaling. Due to this enhancement, the Higgs transitions to light fermions may be observable via the radiative decays despite the smallness of fermion masses. The searches for those Higgs decays are not only to test the consistency of the SM, but also to seek for potential new physics in either the Yukawa or the electroweak sector [8–11]. In the due course, we argue that the quantum electrodynamics (QED) corrections and their effects on the fermion running mass should be taken into account as far as the precision Higgs physics is concerned.

The rest of the paper is organized as follows. We present the full one-loop electroweak corrections to the decay $h \rightarrow f\bar{f}$ in Sec. 2 and show the kinematical features by some differential distributions. We then discuss the observability of the leptonic channels at the LHC in Sec. 3. We finally study the difficult channel $h \rightarrow c\bar{c}\gamma$ in Sec. 4. We summarize our results in Sec. 5.

Fermion	$\bar{m}_f(m_f)$ [GeV]	$\delta\bar{m}_f^{\text{QCD}}$ [GeV]	$\delta\bar{m}_f^{\text{QED}}$ [MeV]	$\bar{m}_f(m_h)$ [GeV]	$\Gamma_{h \rightarrow f\bar{f}}^0$ [keV]
b	4.18	-1.39	-5.72	2.78	1900
c	1.27	-0.657	-9.33	0.604	89.7
τ	1.78	-	-27.2	1.75	251
μ	0.106	-	-4.05	0.102	0.852
e	0.511×10^{-3}	-	-2.20×10^{-2}	0.489×10^{-3}	1.96×10^{-5}

Table 1: The $\overline{\text{MS}}$ running masses with N⁴LO QCD and NLO QED corrections. The last column is the LO width with the running Yukawa coupling effect.

2 $h \rightarrow f\bar{f}(\gamma)$ at One-Loop

It is well known that the tree-level decay width for $h \rightarrow f\bar{f}$ as shown in Fig. 1a is

$$\Gamma_{h \rightarrow f\bar{f}}^0 = \frac{y_f^2 N_c}{16\pi} m_h \beta_f^3, \quad \beta_f = \sqrt{1 - \frac{4m_f^2}{m_h^2}}. \quad (2.1)$$

where, in the SM, the Yukawa coupling is $y_f = \sqrt{2} m_f/v$, and the color factor $N_c = 3$ (1) for a color triplet (singlet) fermion. Quantum chromodynamics (QCD) corrections to the decay of the Higgs to a quark pair have been known up to N⁴LO at $\mathcal{O}(\alpha_s^4)$ [12, 13]. To serve as a comparison with the current work, we write the expression as

$$\Gamma_{\text{NLO QCD}} = \Gamma^0 \left(1 + C_F \frac{\bar{\alpha}_s}{\pi} \frac{17}{4} + \mathcal{O}(\alpha_s^2) \right), \quad \Gamma^0 = \frac{N_c}{8\pi} m_h \frac{\bar{m}_f^2}{v^2} \beta_f^3, \quad (2.2)$$

where $\bar{\alpha}_s^2$ and \bar{m}_f^2 are the renormalized QCD running coupling and quark mass, respectively, to the scale m_h^2 in the $\overline{\text{MS}}$ subtraction scheme, and the color factor $C_F = (N_c^2 - 1)/2N_c = 4/3$. The most significant effect is due to the running of the quark mass from $\mu_0 = m_f$ to $\mu = m_h$ [14–18]. For the sake of illustration and comparison, we only give the one-loop QCD running mass expression as

$$\bar{m}(\mu) = \bar{m}(\mu_0) \left(\frac{\bar{\alpha}_s(\mu)}{\bar{\alpha}_s(\mu_0)} \right)^{\frac{\gamma_0}{b_0}} = \bar{m}(\mu_0) \left(1 + \frac{b_0}{4\pi} \bar{\alpha}_s(\mu_0) \ln \frac{\mu^2}{\mu_0^2} \right)^{-\frac{\gamma_0}{b_0}} \quad (2.3)$$

where $\gamma_0 = 4$ and $b_0 = 11 - 2n_f/3$ in QCD.

2.1 $\mathcal{O}(y_f^2\alpha)$ corrections

Similar to the above, QED corrections to the Higgs radiative decay at $\mathcal{O}(y_f^2\alpha)$, depicted in Figs. 1b–1d, have the same form except for the color factor and the electric charge of the

fermions,

$$\Gamma_{\text{NLO QED}} = \Gamma^0 \left(1 + Q_f^2 \frac{\bar{\alpha}}{\pi} \frac{17}{4} + \mathcal{O}(\alpha^2) \right). \quad (2.4)$$

Therefore, the QED corrections to the partial width at the next-to-leading order (NLO) contribute about $Q_f^2 \times \mathcal{O}(1\%)$ to the Higgs partial width to a fermion pair. Analogous to QCD, we should also take into account the effect of QED running mass, which can be calculated using Eq. (2.3) with $\gamma_0 = 3Q_f^2$ and $b_0 = -4 \sum_f Q_f^2/3$ in QED. This 1-loop running from m_f to m_h will change the fermion mass by about 4% for the electron and about 0.1% (0.8%) for the b -quark (c -quark), comparable to the fix-order QED correction as above. The running mass effect from N⁴LO QCD and NLO QED are summarized in Table 1. The entries in the last column of Table 1 are evaluated with the running Yukawa coupling effects, using the LO partial width formula of Eq. (2.1). We note that the full SM prediction for the Higgs total width is 4.1 MeV [19].

The complete EW corrections to $h \rightarrow f\bar{f}$ partial width at $\mathcal{O}(y_f^2\alpha)$ is

$$\delta\Gamma_{\text{EW}} = \Gamma^0 \left(\frac{2\delta m_f^{\text{QED}}}{\bar{m}_f} + Q_f^2 \frac{\bar{\alpha}}{\pi} \frac{17}{4} + \Delta_{\text{weak}} + \mathcal{O}(\alpha^2) \right), \quad (2.5)$$

where $\delta m_f^{\text{QED}} = \bar{m}(m_h) - \bar{m}(m_f)$ as listed in Table 1, and Δ_{weak} follows the on-shell definition in [20]. The two terms of QED are for mass and vertex corrections and they have opposite signs. The 1-loop EW diagrams as shown in Figs. 1b–1g are all proportional to m_f , and thus we will refer this section as “Yukawa corrections”. We also refer the exclusive real photon emission represented by Fig. 1d as “QED radiation” in later sections.

As the precision of the Higgs measurements improves in the future, it will become necessary to take these corrections into account. In particular, the projected precision of the $hb\bar{b}$ coupling determination was estimated to be 0.3% at the International Linear Collider [21].

2.2 $\mathcal{O}(y_t^2\alpha^3, \alpha^4)$ corrections

Besides the $\mathcal{O}(y_f^2\alpha)$ corrections from the chirality-flipping diagrams governed by the Yukawa couplings, the decay of a Higgs boson to a pair of fermions plus a photon can also be induced by electroweak loops of top quark and gauge bosons. Figure 2 shows some representative electroweak one-loop diagrams. According to their distinctive kinematics and couplings, they can be cast into five classes:

- I. $H \rightarrow \gamma Z^* \rightarrow f\bar{f}\gamma$ (Figs. 2a, 2b)
- II. $H \rightarrow \gamma\gamma^* \rightarrow f\bar{f}\gamma$ (Figs. 2a, 2b)
- III. Z -boson triangle or box with final state radiation (Figs. 2c, 2d)
- IV. W -boson triangle or box with final state radiation (Figs. 2c, 2d, 2e)
- V. top-quark triangle or box with final state radiation (Figs. 2f, 2g, 2h)

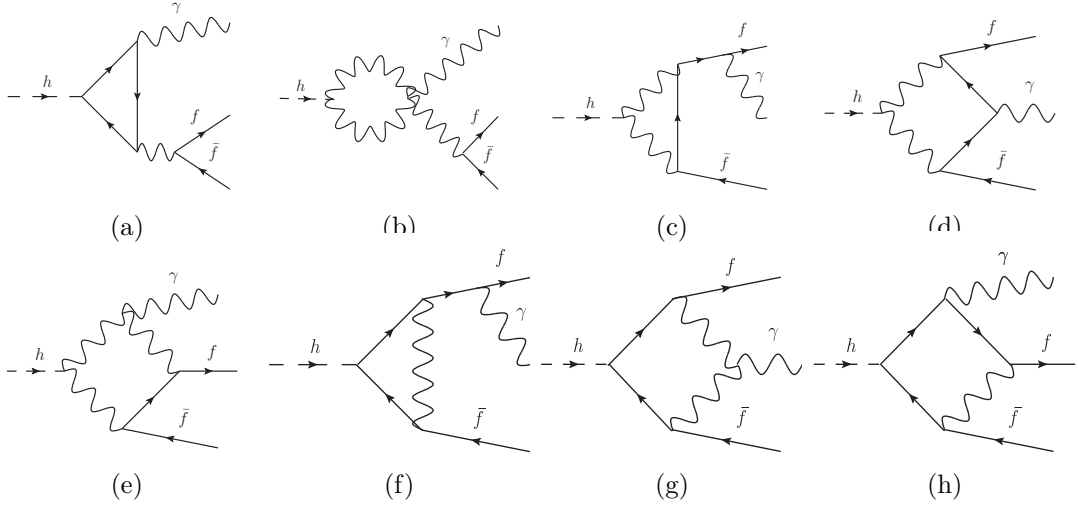


Figure 2: Representative Feynman diagrams of $h \rightarrow f \bar{f} \gamma$ with electroweak one-loop.

We will call them collectively the “EW+ γ ” contributions, distinctive from the chirality-flipping Yukawa corrections in Sec. 2.1. The interference between the QED radiation in Fig. 1d and the EW+ γ processes in Fig. 2 is suppressed by m_f/M_W , as they have different chiral structures for the final state fermions. The EW+ γ loops are UV-finite so that there is no need for renormalization, as pointed out in Ref. [22]. In the massless limit $m_f \rightarrow 0$, the diagrams in Figs. 2a and 2b diverge as the invariant mass of the fermion pair approaches the photon pole $M_{f\bar{f}} \rightarrow 0$. Therefore, a finite fermion mass needs to be kept so that $M_{f\bar{f}}^2 > 4m_f^2$, to regularize the divergent behavior.

We perform the calculation in the Feynman gauge. As a cross check, the analytic results have been calculated and given in [7], where a non-linear R_ξ gauge was used. All the diagrams are generated by *FeynArts* [23], and *FeynCalc* [24] is used to simplify the amplitudes further. The numerical evaluation of all Passarino-Veltman loop integrals [25] are performed by LoopTools [26]. And we use *Vegas* [27] as the phase space integrator.

2.3 Partial decay widths

The Yukawa corrections as in Figs. 1b–1g are of the order $y_f^2 \alpha$, governed by the Yukawa couplings, while the EW+ γ loops in Figs. 2a, 2f–2h, are of the order $y_t^2 \alpha^3$, and the order of α^4 for Figs. 2b–2e. We present our results for these two decay mechanisms in Table 2. The first column shows the NLO EW corrections to the Yukawa interactions as given in Eq. (2.5). The inclusive corrections are small and negative. The second column gives the one-loop EW+ γ contributions at the order of $y_t^2 \alpha^3$ and the order of α^4 , including their interference. The dominant EW+ γ contributions are from diagrams in Figs. 2a and 2b, featured by $\gamma^*, Z \rightarrow f \bar{f}$. The rest of the diagrams is sub-leading and contributing about a few percent. As seen, those contributions from EW+ γ loops are essentially independent of the light fermion masses and thus independent of the Yukawa couplings. The moderate dependence on the mass is due to the kinematical enhancement from the photon splitting near $M_{f\bar{f}} \sim 2m_f$. In comparison with these two decay mechanisms of the Yukawa cor-

	Inclusive corrections		Exclusive decay	
Decay	$\delta\Gamma (y_f^2\alpha)$	$\delta\Gamma (y_t^2\alpha^3, \alpha^4)$	$\Gamma(f\bar{f}\gamma)$ [keV]	$\text{BR}(f\bar{f}\gamma)$ [10^{-4}]
Channels	[keV]	[keV]	$E_\gamma^{\text{cut}} = 5/15$ GeV	$E_\gamma^{\text{cut}} = 5/15$ GeV
$h \rightarrow b\bar{b}$	-25.3	0.99	9.45/5.44	23/13
$h \rightarrow c\bar{c}$	-1.17	0.91	2.48/1.73	6.1/4.2
$h \rightarrow \tau^+\tau^-$	-1.37	0.31	10.4/5.63	25/14
$h \rightarrow \mu^+\mu^-$	-4.72×10^{-2}	0.41	0.436/0.420	1.1/1.0
$h \rightarrow e^+e^-$	-1.29×10^{-6}	0.60	0.589/0.588	1.4/1.4

Table 2: One-loop Yukawa and EW+ γ corrections to Higgs fermionic decays. The first two columns are the inclusive corrections at the order $\mathcal{O}(y_f^2\alpha)$ and at $\mathcal{O}(y_t^2\alpha^3, \alpha^4)$, respectively. The widths and branching fractions for the exclusive decay are shown in the last two columns ($E_\gamma > 5/15$ GeV, and $\Delta R_{f\gamma} > 0.4$).

rections and EW+ γ contributions, we see that the orders of magnitudes are comparable for the $c\bar{c}$ case. The Yukawa corrections dominate over the EW+ γ contributions for the decays to $b\bar{b}$ and $\tau^+\tau^-$, while it becomes the other way around for $\mu^+\mu^-$ and e^+e^- , due to their much smaller Yukawa couplings.

From the observational point of view with the $f\bar{f}\gamma$ events, we require a photon in the final state to satisfy the minimal acceptance cuts¹

$$E_\gamma > 5 \text{ or } 15 \text{ GeV} \quad \text{and} \quad \Delta R_{\gamma f}, \Delta R_{\gamma \bar{f}} > 0.4. \quad (2.6)$$

In Table 2, we list the partial widths and the branching fractions (BR) in the last two columns with a photon satisfying the cuts in Eq. (2.6). We note that the exclusive partial widths of $f\bar{f}\gamma$ can be sizable. The branching fractions of $b\bar{b}\gamma$, $\tau^+\tau^-\gamma$ are of the order of 0.2%, largely from the QED radiation and thus quite sensitive to the photon energy threshold. The branching fraction of $c\bar{c}\gamma$, on the other hand, is about 6×10^{-4} , with comparable contributions from the QED radiation and EW+ γ processes, and thus also rather sensitive to the photon energy cut. Those for $e^+e^-\gamma$ and $\mu^+\mu^-\gamma$ are about 10^{-4} , dominantly from the EW+ γ processes and thus insensitive to the photon energy threshold, to be further discussed below. It is interesting to note that it would be totally conceivable for observation of those clean leptonic channels at the HL-LHC. We also show the Higgs decay branching fractions to fermions in Fig. 3. It is quite informative to compare our results for the exclusive radiative decays $h \rightarrow f\bar{f}\gamma$ with those from $h \rightarrow f\bar{f}$.

¹The kinematical variables here are in the Higgs boson rest-frame. In realistic simulations, one may need to evaluate them in the lab frame.

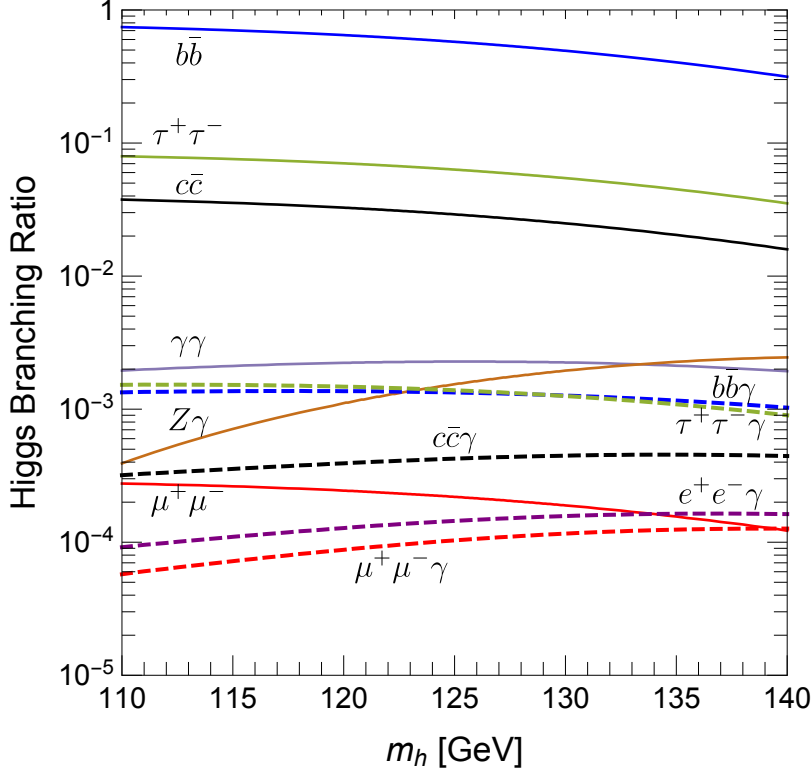


Figure 3: SM Higgs decay branching fractions to fermions with and without the additional photon $E_\gamma > 15$ GeV and $\Delta R > 0.4$.

It is interesting to explore some kinematical distributions to appreciate the underlying decay mechanisms and to guide future experimental searches. In Fig. 4, we show the photon energy distributions in the Higgs boson rest frame for the individual fermionic channels for the QED radiation (solid blue curves) and for the EW+ γ processes (solid red curves) and the total (upper curves). The E_γ spectrum of the QED radiation exhibits the common infrared behavior: the observable photon energy spectrum diverges like dE_γ/E_γ , although the inclusive integrated rate is finite due to the cancelation from the virtual loop diagrams. The energy spectrum of the EW+ γ processes, on the other hand, exhibits a double-hump structure as seen from the red curves in Fig. 4, characterizing the two dominant underlying processes

$$E_\gamma = \frac{m_h}{2} \left(1 - \frac{m_Z^2}{m_h^2}\right) \approx 30 \text{ GeV, for } \gamma Z \text{ production,} \quad (2.7)$$

$$E_\gamma = \frac{m_h}{2} \left(1 - \frac{m_{\gamma^*}^2}{m_h^2}\right) \approx 63 \text{ GeV, for } \gamma\gamma^* \text{ production.} \quad (2.8)$$

The diagrams of Figs. 2c and 2e have a spurious divergence in the infrared (soft) and collinear region. However, in the soft/collinear limit, the amplitude has to be proportional to the fermion mass due to conservation of angular momentum, and thus vanishes in the massless limit, as confirmed by the plots here.

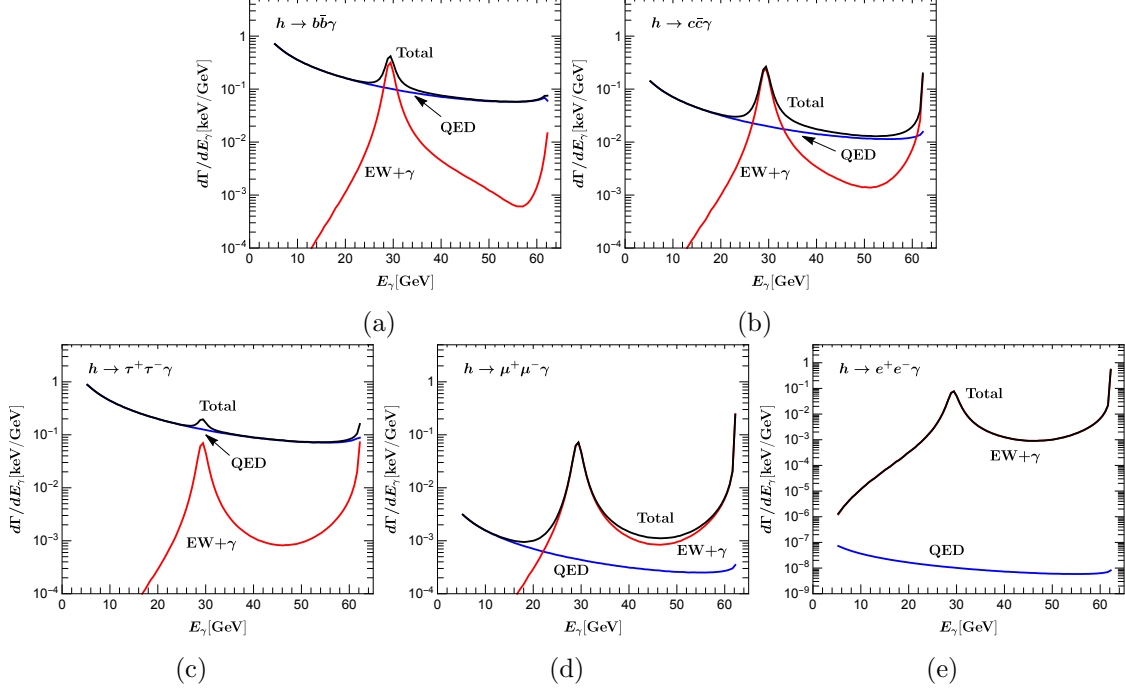


Figure 4: The photon energy distributions in $h \rightarrow f\bar{f}\gamma$ ($f = b, c, \tau, \mu, e$) in the Higgs boson rest frame. The blue curves are for the QED radiation (Fig. 1d); the red curves are for the EW+ γ processes (Fig. 2); the upper black lines are for the total.

We also show the invariant mass distributions of the fermion pairs in Fig. 5. Generally speaking, there is a correlation between the invariant mass and the energy as $M_{ff}^2 = m_h^2 - 2m_h E_\gamma$. While the invariant mass spectrum of the QED radiation has a rather smooth distribution, those from EW+ γ processes are again seen with the double-humps, one near the Z -pole and another near $m_{\gamma^*} \sim 2m_f$, which becomes more pronounced for a smaller fermion mass. This is the reason why the decay rate for $e^+e^-\gamma$ is larger than that for $\mu^+\mu^-\gamma$.

Finally, we show in Fig. 6 the distributions of the photon separation from the fermions, defined in the pseudo rapidity-azimuthal angle space $\Delta R_{\gamma f} = (\Delta\eta^2 + \Delta\phi^2)^{1/2}$. As expected, the QED radiation exhibit a collinear divergence near $\Delta R_{\gamma f} \rightarrow 0$, and the EW+ γ processes lead to a back-to-back structure $\Delta R_{\gamma f} \rightarrow \pi$.

3 LHC Search for $\ell^+\ell^-\gamma$

In the upcoming and future LHC programs, it is of fundamental importance to observe the Higgs boson rare decays to check the consistency of the SM and seek for hints for new physics. Given the anticipated large yield at the HL-LHC, reaching about 150 million Higgs bosons, the very clean final states $\ell^+\ell^-\gamma$ ($\ell = \mu, e$) should be among the first to look for. We now discuss their observability at the LHC.

As mentioned in Sec. 2.3, the radiative decays $h \rightarrow \mu^+\mu^-\gamma$ and $h \rightarrow e^+e^-\gamma$ are mainly from the chirality-conserving EW+ γ loop diagrams. As seen from Figs. 5d and 5e, the

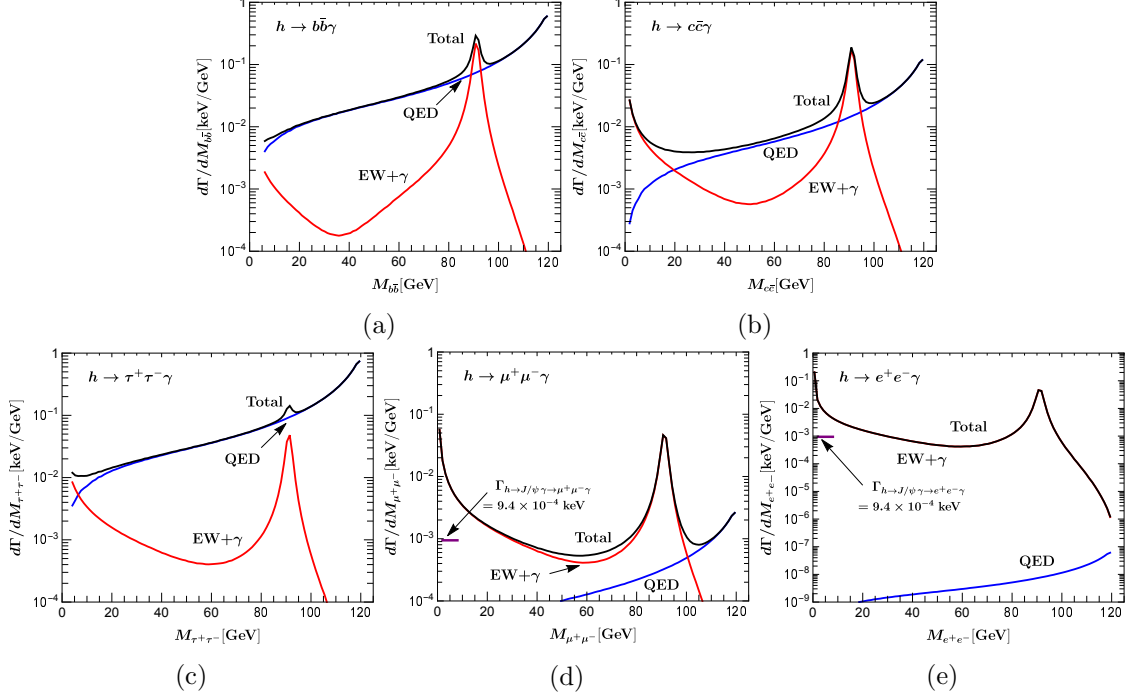


Figure 5: The invariant mass distributions of the fermion pair in $h \rightarrow f\bar{f}\gamma$ ($f = b, c, \tau, \mu, e$). The blue curves are for the QED radiation (Fig. 1d); the red curves are for the EW+ γ processes (Fig. 2); the upper black lines are for the total. The decay widths for the channels $h \rightarrow J\psi \gamma \rightarrow \ell^+\ell^-\gamma$ are indicated by the horizontal bars in (d) and (e), in units of keV without the photon acceptance cuts.

leading contributions are from $h \rightarrow \gamma^*\gamma, Z\gamma \rightarrow \ell^+\ell^-\gamma$ [28–31]. It is thus a good search strategy to focus on the γ -pole and the Z -pole. Some searches have been carried out by ATLAS [32] and CMS [33, 34] at the 7–8 TeV LHC. We present our analyses below in the hope to serve as a theoretical guidance for the future experimental searches at the LHC. We focus on the leading production for the Higgs boson via the gluon fusion. The QCD corrections are taken into account by multiplying a flat NNLO QCD K -factor of $K = 2.7$ for the gluon fusion [35]. The dominant SM background is the Drell-Yan production of the lepton pair $\ell^+\ell^-$ with an initial/final state photon radiation. We calculate the background processes at LO using *MadGraph* [36], and then multiplied by flat QCD K -factors $K = 1.4$ for $pp \rightarrow Z\gamma \rightarrow \ell^+\ell^-\gamma$ [37], and $K = 6.2$ for $pp \rightarrow \gamma^*\gamma \rightarrow \ell^+\ell^-\gamma$ [38].

3.1 $h \rightarrow \gamma^*\gamma \rightarrow \ell^+\ell^-\gamma$

To make the close connection with the LHC searches, we first follow the event selection cuts adopted by the CMS collaboration [34]. As the invariant mass of the lepton pair approaches to $2m_f$, the lepton pair tends to be collimated. This becomes particularly challenging for the electron channel, because the electron pair merges into one supercluster. Therefore, a single muon plus a photon trigger for the muon channel and a di-photon trigger for the electron channel are implemented. To select the signal events near the γ -pole from the

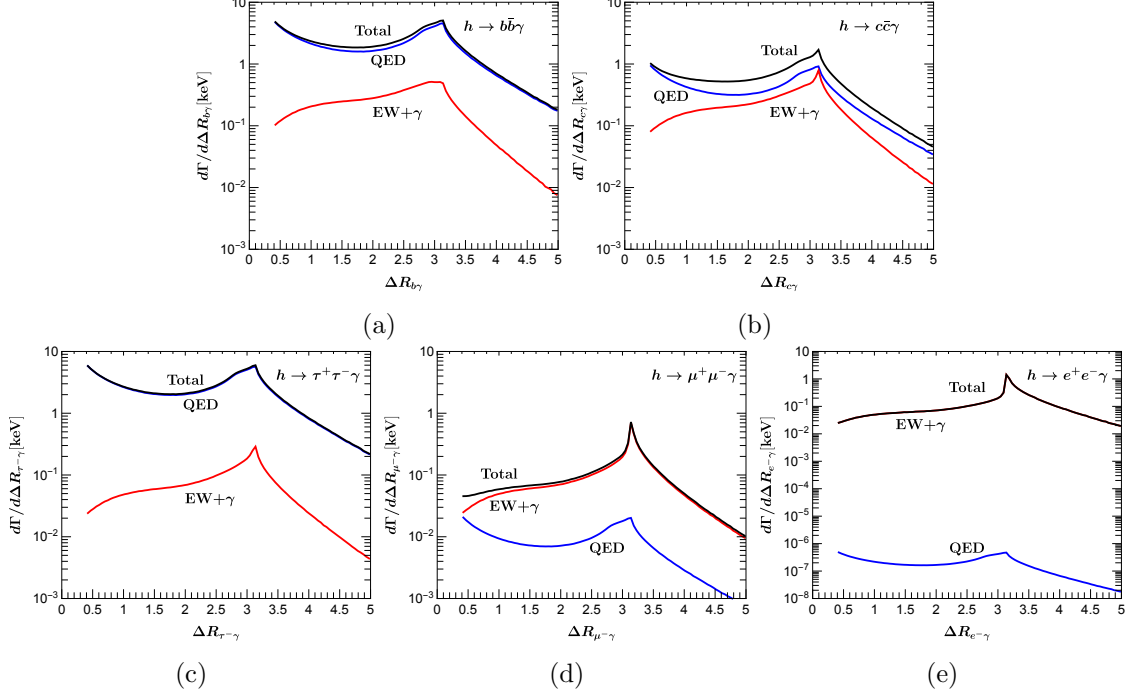


Figure 6: The distributions of the photon separation from the fermions in $h \rightarrow f\bar{f}\gamma$ ($f = b, c, \tau, \mu, e$) in the Higgs boson rest frame. The blue curves are for the QED radiation (Fig. 1d); the red curves are for the EW+ γ processes (Fig. 2); the upper black lines are for the total.

Higgs decay and effectively suppress the backgrounds, we require the invariant masses to be

$$M_{\mu\mu} < 20 \text{ GeV}, \quad M_{ee} < 1.5 \text{ GeV}, \quad 120 \text{ GeV} < M_{\ell\ell\gamma} < 130 \text{ GeV}. \quad (3.1)$$

The leading (sub-leading) muon must satisfy the acceptance of the transverse momentum and pseudo-rapidity

$$p_T^\mu > 23 \text{ (4) GeV}, \quad |\eta_\mu| < 2.4. \quad (3.2)$$

The electrons must satisfy

$$|p_{Te^+}| + |p_{Te^-}| > 44 \text{ GeV}, \quad |\eta_e| < 1.44. \quad (3.3)$$

so that a multivariate discriminator can be used to separate $\gamma^* \rightarrow e^+e^-$ from jets or single electrons [34].² The photon must satisfy the following acceptance and be well-separated from leptons

$$p_T^\gamma > 0.3M_{\ell\ell}, \quad |\eta_\gamma| < 1.44, \quad \Delta R_{\gamma\ell} > 1. \quad (3.4)$$

We would like to point out that, given the well-predicted kinematical properties of a fully reconstructable decay of the Higgs boson, the analyses may be improved by further utilizing

²CMS trained a discriminator to identify electron pairs. We did not include this treatment in our simulations.

the signal kinematical features. One of striking features is the mono-chromatic nature of the photon as given in Eqs. (2.7) and (2.8). We thus propose to tighten the Higgs mass cut in Eq. (3.1) as much as experimentally feasible, then boost the system to the Higgs boson rest frame, and impose the following cuts

$$60 < E_\gamma < 63 \text{ GeV in the rest frame of } \ell\ell\gamma, \quad (3.5)$$

Another alternative option is to tighten the transverse momentum cut on the photon,

$$p_T^\gamma > 55 \text{ GeV}. \quad (3.6)$$

The comparison of different cuts are demonstrated in Table 3, where the cross sections of signals and backgrounds, as well as the statistical significances are listed. Due to the stronger enhancement near the photon pole $\gamma^* \rightarrow e^+e^-$, one would be able to reach a $4.5\sigma/14\sigma$ sensitivity for the channel $h \rightarrow e^+e^-\gamma$ at the LHC with an integrated luminosity $0.3 \text{ ab}^{-1}/3 \text{ ab}^{-1}$, and a $3.1\sigma/9.9\sigma$ for the channel $h \rightarrow \mu^+\mu^-\gamma$. It is interesting to compare our results for the radiative decay $h \rightarrow \mu^+\mu^-\gamma$ with the ATLAS projection [39] for the direct decay $h \rightarrow \mu^+\mu^-$ with the sensitivity reach of $2.3\sigma/7.0\sigma$ for $0.3 \text{ ab}^{-1}/3 \text{ ab}^{-1}$. Similar results have also been obtained by the CMS collaboration [40].

3.2 $h \rightarrow Z\gamma \rightarrow \ell^+\ell^-\gamma$

To select the signal events near the Z -pole from the Higgs decay and effectively suppress the backgrounds, we first follow the CMS analysis [33] and require the invariant masses of the final state particles to be

$$M_{\ell\ell} > 50 \text{ GeV}, \quad 120 \text{ GeV} < M_{\ell\ell\gamma} < 130 \text{ GeV}. \quad (3.7)$$

The leading (sub-leading) lepton must satisfy the acceptance of the transverse momentum and pseudo-rapidity

$$p_T^\ell > 20 \text{ (10) GeV}, \quad |\eta_\mu| < 2.5, \quad |\eta_e| < 2.4. \quad (3.8)$$

The photon must satisfy the following acceptance and be well-separated from leptons³

$$p_T^\gamma > 15 \text{ GeV}, \quad |\eta_\gamma| < 2.5, \quad \Delta R_{\gamma\ell} > 0.4. \quad (3.9)$$

Similarly to the $h \rightarrow \gamma^*\gamma \rightarrow \ell^+\ell^-\gamma$ study, we again propose to tighten the energy and momentum cuts

$$27 < E_\gamma < 33 \text{ GeV in the rest frame of } \ell\ell\gamma, \quad (3.10)$$

$$p_T^\gamma > 25 \text{ GeV}, \quad (3.11)$$

as listed in Table 3. Although the tight cuts do not improve the statistical significance significantly for these channels, the signal-to-background ratios are improved by about a

³We also impose $1.44 < |\eta| < 1.57$ to simulate the CMS barrel-end cap transition region. Additional cuts from CMS $p_T^\gamma > (15/110)M_{\ell\ell\gamma}$ and $M_{\ell\ell\gamma} + M_{\ell\ell} > 185 \text{ GeV}$ have been also adopted.

Channel	Signal [fb]	Background [fb]	Statistical Significance with 0.3 (3) ab^{-1} luminosity
$pp \rightarrow \gamma^* \gamma \rightarrow \mu^+ \mu^- \gamma$	0.69	23.5	2.47 (7.79)
$60 < E_\gamma < 63 \text{ GeV}$	0.69	14.6	3.13 (9.89)
$p_{T\gamma} > 55 \text{ GeV}$	0.46	11.8	2.32 (7.33)
$pp \rightarrow \gamma^* \gamma \rightarrow e^+ e^- \gamma$	1.06	27.0	3.53 (11.2)
$60 < E_\gamma < 63 \text{ GeV}$	1.06	17.0	4.45 (14.1)
$p_{T\gamma} > 55 \text{ GeV}$	0.79	17.6	3.26 (10.3)
$pp \rightarrow Z \gamma \rightarrow \mu^+ \mu^- \gamma$	1.40	214	1.66 (5.24)
$27 < E_\gamma < 33 \text{ GeV}$	1.10	121	1.73 (5.48)
$p_{T\gamma} > 25 \text{ GeV}$	0.91	95.9	1.61 (5.09)
$pp \rightarrow Z \gamma \rightarrow e^+ e^- \gamma$	1.38	224	1.60 (5.05)
$27 < E_\gamma < 33 \text{ GeV}$	1.13	126	1.74 (5.51)
$p_{T\gamma} > 25 \text{ GeV}$	0.91	100	1.58 (4.98)

Table 3: The cross sections of signals and backgrounds, and the statistical significances of $pp \rightarrow V \gamma \rightarrow \ell^+ \ell^- \gamma$, $V = Z, \gamma^*$.

factor of two, reaching a 1% level. This would help to keep potential systematic errors in better control. Unlike the γ -pole feature discussed above, there is no appreciable difference between $e^+ e^-$ and $\mu^+ \mu^-$ channels. One would be able to reach a $1.7\sigma/5.5\sigma$ sensitivity at the LHC with an integrated luminosity $0.3 \text{ ab}^{-1}/3 \text{ ab}^{-1}$. Although weaker signals than the $\gamma^* \gamma$ channels above, these will significantly improve the overall observability for $h \rightarrow \ell^+ \ell^- \gamma$ if the analyses can be combined.

3.3 $h \rightarrow J/\psi \gamma \rightarrow \ell^+ \ell^- \gamma$

With respect to another similar final state from the Higgs boson decay, a comparative remark is in order. It has been pointed out that the Higgs rare decay to a photon associated with a heavy vector meson J/ψ may provide the direct access to the charm-Yukawa coupling via the clean leptonic decay channels [41]. The branching fraction in the SM is predicted [42–44] to be

$$\text{BR}_{\text{SM}}(h \rightarrow J/\psi \gamma) = 2.79 \times 10^{-6} \quad \text{and} \quad \text{BR}_{\text{SM}}(h \rightarrow J/\psi \gamma \rightarrow \mu^+ \mu^- \gamma) = 2.3 \times 10^{-7}, \quad (3.12)$$

which is very small. Furthermore, the “direct contribution” involving the charm-Yukawa coupling is much smaller than that from the “indirect contribution” via $\gamma^* \rightarrow J/\psi$ [42],

making the probe to the charm-Yukawa coupling in this channel extremely challenging.

Nevertheless, for comparison, this result has been marked in Figs. 5d and 5e, in units of keV and without the photon acceptance cuts. The superb muon pair mass resolution of the order 100 MeV would be needed in order to have a chance to dig out the weak signal from the continuum $h \rightarrow \gamma^* \gamma \rightarrow \ell^+ \ell^- \gamma$ events, on top of the other SM background sources. We propose to start with the larger event samples of $\ell^+ \ell^- \gamma$ as discussed in the last two sections, relax the J/ψ -specific cuts in the hope for an early observation of the $h \rightarrow \ell^+ \ell^- \gamma$ signal, and then to extend the search to scrutinize the potential excess from $J/\psi \rightarrow \ell^+ \ell^-$.

Dedicated searches for this decay channel have been performed by ATLAS [45] and CMS [34]. With 20 fb^{-1} luminosity, both ATLAS and CMS set a bound of $\text{BR}(h \rightarrow J/\psi \gamma) < 1.5 \times 10^{-3}$ under the assumption of SM Higgs production. If the BSM physics only enhances the charm-Yukawa coupling by a factor of κ_c ,

$$y_c^{\text{BSM}} = \kappa_c y_c^{\text{SM}}, \quad (3.13)$$

then this experimental bound can be translated into a loose bound on $\kappa_c \lesssim 220$ [46]. With 3 ab^{-1} luminosity at the HL-LHC, the expected upper limit to $\text{BR}_{\text{SM}}(h \rightarrow J/\psi \gamma)$ is about 15 times the SM value [47], which corresponds to a upper bound of about $\kappa_c \lesssim 50$.

3.4 $h \rightarrow \tau^+ \tau^- \gamma$

Besides the clean $e^+ e^- \gamma$, $\mu^+ \mu^- \gamma$ final states, the $\tau^+ \tau^- \gamma$ channel is also of considerable interests from the observational point of view. The direct decay $h \rightarrow \tau^+ \tau^-$ has been observed in the LHC experiments mainly via the vector-boson-fusion production mechanism [3, 6]. The radiative decay channel $h \rightarrow \tau^+ \tau^- \gamma$ may be searched for via the leading production channel of gluon fusion. To compare the rates, we have at the 14 TeV LHC,

$$\sigma(WW, ZZ \rightarrow h \rightarrow \tau^+ \tau^-) = (4.2 \text{ pb}) \times (6.3\%) \approx 260 \text{ fb}; \quad (3.14)$$

$$\sigma(gg \rightarrow h \rightarrow \tau^+ \tau^- \gamma) = (49 \text{ pb}) \times (0.1\%) \approx 50 \text{ fb}. \quad (3.15)$$

Thus, it is quite conceivable to observe this radiative decay mode in the future searches. The kinematical features of this decay will be rather different from those presented in the last sections due to the dominance of the QED radiation. Because of the complexity of the tau decay final states, the signal observation and the background suppression will need to be carefully analyzed. We will leave this to a future analysis.

4 LHC Search for $c\bar{c}\gamma$ and the Charm-Yukawa Coupling

It is crucially important to search for the decay $h \rightarrow c\bar{c}$ since it is the largest mode for the Higgs boson to couple to the second generation fermions, and it may be sensitive to physics beyond the Standard Model [48–58]. Given the difficulty as seen above in searching for $h \rightarrow J/\psi \gamma \rightarrow \ell^+ \ell^- \gamma$, other methods have also been explored to probe the charm-Yukawa coupling [59–65]. In this section, we discuss the possibility of constraining the charm-Yukawa coupling using the open-flavor channel $pp \rightarrow c\bar{c}\gamma$, which has a much larger branching fraction about 4×10^{-4} , as seen in Fig. 3. The additional photon radiation may

Operating Point	ϵ_c	ϵ_b	ϵ_j
I	20%	10%	1%
II	30%	20%	3%
III	45%	50%	10%

Table 4: Representative operating points for the c -tagging efficiency (ϵ_c), b and light jets contamination rates (ϵ_b and ϵ_j).

Luminosity	Operating Point	Signal (Total)	Signal (QED)	Signal (EW+ γ)	Background
3000 fb^{-1}	I	778	252	492	3.84×10^7
	II	1750	567	1107	1.25×10^8
	III	3937	1275	2491	6.51×10^8

Table 5: Numbers of events for the signals and backgrounds with the three c -tag operating points for an integrated luminosity of 3000 fb^{-1} .

serve as the trigger and is in favor of picking out the $c\bar{c}$ events over $b\bar{b}$ due to the larger charm electric charge.

The signal events are characterized by a high- p_T photon recoiling against a pair of charm-jets. To identify such events, an efficient charm-tagging technique is required. Although currently there is no dedicated charm-tagging being implemented at the LHC, the discrimination of a c -jet from a b -jet has been studied and used in the calibration of the b -tagging efficiency [66, 67]. ATLAS also proposed a c -tagging algorithm [68] based on the neural network that could achieve about 20% (90%) tagging efficiency with a medium (loose) cut criteria in the search for $pp \rightarrow \tilde{t}\tilde{t}^* \rightarrow (c\tilde{\chi}_1^0)(c\tilde{\chi}_1^0)$. In the current study, we choose three representative operating points listed in Table 4, for the c -tagging efficiency ϵ_c , and b and light jets contamination rates, ϵ_b and ϵ_j , respectively. When increasing the c -tagging efficiency from I to III, we must accept higher contaminations from a heavier quark and light jets.

The dominant background is the QCD di-jet plus a direct photon production, with the jets to be mis-tagged as c -jets. Another major background is the QCD 3-jet production, leading to two mis-tagged c -jets associated with a fake photon radiation. Following an ATLAS analysis [69], we take the photon fake rate from a light-quark jet and from a gluon jet to be

$$\epsilon_{q \rightarrow \gamma} = 0.06\%, \quad \epsilon_{g \rightarrow \gamma} = 0.006\%, \quad (4.1)$$

Method	κ_c upper limit projection at HL-LHC (3 ab ⁻¹)
$h \rightarrow c\bar{c}\gamma$ (this work)	6.3
$h \rightarrow c\bar{c}$ +fit [61]	2.5
$h + c$ production [62]	2.6
Higgs kinematics [63]	4.2
$h \rightarrow J/\psi\gamma$ [47]	50

Table 6: Projected sensitivities for probing the $hc\bar{c}$ Yukawa coupling $\kappa_c = y_c^{\text{BSM}}/y_c^{\text{SM}}$ at the HL-LHC with various methods.

respectively. We note that the fake photon contamination contributes about (10–30)% to the total background. Another potentially large background is from jet fragmentation into a real photon. We assume that the stringent photon isolation requirement will be sufficient to suppress this QCD background, as pointed out in the prompt photon studies [70]. In our simulations, we require that both the c -jets and the photon be hard and well-isolated in the central region

$$p_T > 20 \text{ GeV}, \quad |\eta| < 2.5, \quad \text{and} \quad \Delta R > 0.4. \quad (4.2)$$

The ultimate sensitivity for the signal $h \rightarrow c\bar{c}\gamma$ depends on the invariant mass reconstruction $M_{jj\gamma} = m_h$, and thus the energy resolution of the charm-jets. In this study, we assume that the Higgs resonance peak can be reconstructed within 20% and thus we require

$$100 \text{ GeV} < M_{jj\gamma} < 150 \text{ GeV}. \quad (4.3)$$

Tightening this mass cut would linearly improve the signal-to-background ratio. We also apply $p_T^{\text{max}} > 40 \text{ GeV}$ to further increase the signal-to-background ratio S/B . After the above cuts applied, we list the numbers of events in Table 5 for an integrated luminosity of 3000 fb⁻¹. We note that, within the SM, the signal events from the QED radiation and the EW+ γ processes are comparable, unlike the situation in $h \rightarrow J/\psi \gamma$ where the dominant contribution is from the “indirect contribution” via $\gamma^* \rightarrow J/\psi$. Unfortunately, with the Standard Model predictions for the signal and backgrounds being $S/B < 10^{-4}$, it would not be promising to observe this channel at the HL-LHC.

If the BSM physics significantly modifies the charm-Yukawa coupling as parameterized in Eq. (3.13), then the QED radiation will be scaled by a factor of κ_c^2 . Although both the QED radiation and EW+ γ processes contribute to the signal, it would be dominated by the QED radiation if the charm-Yukawa coupling significantly deviates from the SM value. Therefore, considering only the statistical significance by the Gaussian standard deviation

$$\sigma_{\text{SD}} = \frac{N_S^{\text{BSM}}}{\sqrt{N_B}} \simeq \frac{\kappa_c^2 N_S^{\text{QED}}}{\sqrt{N_B}}, \quad (4.4)$$

the 2σ -bounds on the charm-Yukawa coupling are obtained as

$$\kappa_c < 12.5 \text{ (7.0)}, \quad 11.1 \text{ (6.3)}, \quad 11.2 \text{ (6.3)}. \quad (4.5)$$

for operating points I, II, III with a luminosity of 3000 fb^{-1} . Those results with the Higgs radiative decay, although still rather weak, could be comparable to the recent studies on the charm-Yukawa coupling [61–63, 65] and seem to be more advantageous to $h \rightarrow J/\psi \gamma$. We have compiled the existing results in Table 6. The first three methods listed here rely on different production mechanisms and certain charm-tagging techniques with various assumptions of c -tagging efficiencies.⁴ Nevertheless, they tend to have better performances than the $h \rightarrow J/\psi \gamma$ channel, mainly because of the larger signal rates for the open c -flavor production. Those channels should thus be complementary in the future explorations.

5 Summary

Given the current null results on BSM searches at the LHC, it is strongly motivated to search for rare decays of the Higgs boson to test the Higgs sector in the SM and to seek for hints of BSM physics. In this work, we studied the Higgs rare decay channels $h \rightarrow f \bar{f} \gamma$ where $f = \tau, \mu, e$ and b, c and their observability at the LHC. Our results can be summarized as follows.

- This radiative decay channel receives contributions from QED corrections to the Yukawa interactions at $\mathcal{O}(y_f^2 \alpha)$ and EW+ γ processes at $\mathcal{O}(y_t^2 \alpha^3, \alpha^4)$, as we discussed in Sec. 2.1 and 2.2. The QED corrections constitute about $Q_f^2 \times \mathcal{O}(1\%)$ to the partial widths of fermionic Higgs decays in particular through the running mass, and therefore should be taken into account for future precision Higgs physics.
- As showed in Sec. 2.3, the contributions from the Yukawa corrections (Fig. 1) and the EW+ γ contributions (Fig. 2) exhibit quite different patterns for different fermions in the final state: While they are comparable for $c\bar{c}\gamma$, the Yukawa corrections dominate for $b\bar{b}\gamma$, $\tau^+\tau^-\gamma$. The EW+ γ loops overwhelm for $\mu^+\mu^-\gamma$, $e^+e^-\gamma$, which results in the branching fractions of the order $\mathcal{O}(10^{-4})$ despite their tiny Yukawa couplings (see Fig. 3). The main contributions in the EW+ γ loops are around the Z -pole, as well as the γ -pole near $m_{\gamma^*} \approx 2m_f$. The kinematic distributions, especially the photon energy distributions in Fig. 4 and the invariant mass distributions in Fig. 5 are quite informative to reveal the underlying decay mechanisms, and to guide the experimental searches.
- As the $e^+e^-\gamma$ and $\mu^+\mu^-\gamma$ channels exhibit the violation of the Yukawa scaling, we studied their observability at the LHC in Sec. 3, taking into account the signal characteristics and the SM background. We conclude that, with an integrated luminosity $0.3 \text{ ab}^{-1}/3 \text{ ab}^{-1}$, the channels $h \rightarrow \gamma^* \gamma \rightarrow e^+e^-\gamma$ ($\mu^+\mu^-\gamma$) should be observable at the level of $4.5\sigma/14\sigma$ ($3.1\sigma/9.9\sigma$), and the channels $h \rightarrow Z\gamma \rightarrow e^+e^-\gamma$, $\mu^+\mu^-\gamma$ should be observable at the level of $1.5\sigma/5.5\sigma$. The sensitivity could be comparable to the direct search of the two-body decay $h \rightarrow \mu^+\mu^-$.

⁴The authors in [61] used an integrated luminosity of $2 \times 3000 \text{ fb}^{-1}$ (combining both the ATLAS and CMS data), and the tagging efficiencies $\epsilon_c = 0.5$, $\epsilon_b = 0.2$, and $\epsilon_j = 0.005$; while the authors in [62] adopted the tagging efficiencies $\epsilon_c = 0.4$, $\epsilon_b = 0.3$, and $\epsilon_j = 0.01$. If using their choices for our analysis, we would have gotten a slightly stronger bound with $\kappa_c < 4.2$ and 4.9 , respectively.

- The decay $h \rightarrow J/\psi \gamma \rightarrow \ell^+ \ell^- \gamma$ has the same final state but much smaller rate. The searches for the above channels will serve as the necessary early discovery and will shed light on the potential observation for $h \rightarrow J/\psi \gamma$.
- In Sec. 3.4, we pointed out a potentially observable decay $h \rightarrow \tau^+ \tau^- \gamma$. We proposed the search via the leading production mechanism from gluon fusion with the help of the additional photon.
- In Sec. 4, we proposed to probe the charm-Yukawa coupling via the decay channel $h \rightarrow c \bar{c} \gamma$. With the help of future c -tagging techniques, we demonstrated that the charm-Yukawa coupling y_c can be bounded as $y_c^{\text{BSM}} \lesssim 6 y_c^{\text{SM}}$ at 2σ level at the HL-LHC. We find it comparable to the other related studies in the literature, and better than the $J/\psi \gamma$ channel in constraining the charm-Yukawa coupling.

Acknowledgments

We would like to thank Kaoru Hagiwara and Ayres Freitas for helpful discussions. This work is supported in part by the Department of Energy under Grant No. DE-FG02-95ER40896 and in part by PITT PACC. XW was also supported in part by a PITT PACC Predoctoral Fellowship from School of Arts and Sciences at the University of Pittsburgh.

References

- [1] ATLAS collaboration, T. A. collaboration, *Search for the Standard Model Higgs boson produced in association with top quarks and decaying to $b\bar{b}$ in pp collisions at $\sqrt{s} = 8$ TeV with the ATLAS detector at the LHC*, .
- [2] ATLAS collaboration, G. Aad et al., *Search for the $b\bar{b}$ decay of the Standard Model Higgs boson in associated $(W/Z)H$ production with the ATLAS detector*, *JHEP* **01** (2015) 069, [[1409.6212](#)].
- [3] ATLAS collaboration, G. Aad et al., *Evidence for the Higgs-boson Yukawa coupling to tau leptons with the ATLAS detector*, *JHEP* **04** (2015) 117, [[1501.04943](#)].
- [4] CMS collaboration, V. Khachatryan et al., *Search for the associated production of the Higgs boson with a top-quark pair*, *JHEP* **09** (2014) 087, [[1408.1682](#)].
- [5] CMS collaboration, S. Chatrchyan et al., *Search for the standard model Higgs boson produced in association with a W or a Z boson and decaying to bottom quarks*, *Phys. Rev.* **D89** (2014) 012003, [[1310.3687](#)].
- [6] CMS collaboration, S. Chatrchyan et al., *Evidence for the 125 GeV Higgs boson decaying to a pair of τ leptons*, *JHEP* **05** (2014) 104, [[1401.5041](#)].
- [7] A. Abbasabadi, D. Bowser-Chao, D. A. Dicus and W. W. Repko, *Radiative Higgs boson decays $H \rightarrow \text{fermion anti-fermion gamma}$* , *Phys. Rev.* **D55** (1997) 5647–5656, [[hep-ph/9611209](#)].
- [8] C.-S. Li, C.-F. Qiao and S.-H. Zhu, *Radiative Higgs boson decays $H \rightarrow f \text{ anti-}f \text{ gamma}$ beyond the standard model*, *Phys. Rev.* **D57** (1998) 6928–6933, [[hep-ph/9801334](#)].

- [9] A. Arhrib, R. Benbrik and T.-C. Yuan, *Associated Production of Higgs at Linear Collider in the Inert Higgs Doublet Model*, *Eur. Phys. J. C* **74** (2014) 2892, [[1401.6698](#)].
- [10] S. L. Hu, N. Liu, J. Ren and L. Wu, *Revisiting Associated Production of 125 GeV Higgs Boson with a Photon at a Higgs Factory*, *J. Phys. G* **41** (2014) 125004, [[1402.3050](#)].
- [11] G. Belanger, V. Bizouard and G. Chalons, *Boosting Higgs boson decays into gamma and a Z in the NMSSM*, *Phys. Rev. D* **89** (2014) 095023, [[1402.3522](#)].
- [12] A. Djouadi, *The Anatomy of electro-weak symmetry breaking. I: The Higgs boson in the standard model*, *Phys. Rept.* **457** (2008) 1–216, [[hep-ph/0503172](#)].
- [13] P. A. Baikov, K. G. Chetyrkin and J. H. Kuhn, *Scalar correlator at $O(\alpha_s^4)$, Higgs decay into b-quarks and bounds on the light quark masses*, *Phys. Rev. Lett.* **96** (2006) 012003, [[hep-ph/0511063](#)].
- [14] E. Braaten and J. P. Leveille, *Higgs Boson Decay and the Running Mass*, *Phys. Rev. D* **22** (1980) 715.
- [15] N. Sakai, *Perturbative QCD Corrections to the Hadronic Decay Width of the Higgs Boson*, *Phys. Rev. D* **22** (1980) 2220.
- [16] T. Inami and T. Kubota, *Renormalization Group Estimate of the Hadronic Decay Width of the Higgs Boson*, *Nucl. Phys. B* **179** (1981) 171–188.
- [17] S. G. Gorishnii, A. L. Kataev and S. A. Larin, *The Width of Higgs Boson Decay Into Hadrons: Three Loop Corrections of Strong Interactions*, *Sov. J. Nucl. Phys.* **40** (1984) 329–334.
- [18] M. Drees and K.-i. Hikasa, *NOTE ON QCD CORRECTIONS TO HADRONIC HIGGS DECAY*, *Phys. Lett. B* **240** (1990) 455.
- [19] LHC HIGGS CROSS SECTION WORKING GROUP collaboration, D. de Florian et al., *Handbook of LHC Higgs Cross Sections: 4. Deciphering the Nature of the Higgs Sector*, [1610.07922](#).
- [20] B. A. Kniehl, *Higgs phenomenology at one loop in the standard model*, *Phys. Rept.* **240** (1994) 211–300.
- [21] M. E. Peskin, *Estimation of LHC and ILC Capabilities for Precision Higgs Boson Coupling Measurements*, in *Proceedings, Community Summer Study 2013: Snowmass on the Mississippi (CSS2013): Minneapolis, MN, USA, July 29-August 6, 2013*, 2013. [1312.4974](#).
- [22] A. Abbasabadi, D. Bowser-Chao, D. A. Dicus and W. W. Repko, *Higgs photon associated production at $e\bar{e}$ colliders*, *Phys. Rev. D* **52** (1995) 3919–3928, [[hep-ph/9507463](#)].
- [23] T. Hahn, *Generating Feynman diagrams and amplitudes with FeynArts 3*, *Comput. Phys. Commun.* **140** (2001) 418–431, [[hep-ph/0012260](#)].
- [24] R. Mertig, M. Bohm and A. Denner, *FEYN CALC: Computer algebraic calculation of Feynman amplitudes*, *Comput. Phys. Commun.* **64** (1991) 345–359.
- [25] G. Passarino and M. J. G. Veltman, *One Loop Corrections for e^+e^- Annihilation Into $\mu^+\mu^-$ in the Weinberg Model*, *Nucl. Phys. B* **160** (1979) 151–207.
- [26] T. Hahn and M. Perez-Victoria, *Automatized one loop calculations in four-dimensions and D-dimensions*, *Comput. Phys. Commun.* **118** (1999) 153–165, [[hep-ph/9807565](#)].
- [27] T. Hahn, *CUBA: A Library for multidimensional numerical integration*, *Comput. Phys. Commun.* **168** (2005) 78–95, [[hep-ph/0404043](#)].

- [28] L.-B. Chen, C.-F. Qiao and R.-L. Zhu, *Reconstructing the 125 GeV SM Higgs Boson Through $\ell\bar{\ell}\gamma$* , *Phys. Lett. B* **726** (2013) 306–311, [[1211.6058](#)].
- [29] G. Passarino, *Higgs Boson Production and Decay: Dalitz Sector*, *Phys. Lett. B* **727** (2013) 424–431, [[1308.0422](#)].
- [30] Y. Sun, H.-R. Chang and D.-N. Gao, *Higgs decays to $\gamma\ell^+\ell^-$ in the standard model*, *JHEP* **05** (2013) 061, [[1303.2230](#)].
- [31] A. Yu. Korchin and V. A. Kovalchuk, *Angular distribution and forward–backward asymmetry of the Higgs-boson decay to photon and lepton pair*, *Eur. Phys. J. C* **74** (2014) 3141, [[1408.0342](#)].
- [32] ATLAS collaboration, G. Aad et al., *Search for Higgs boson decays to a photon and a Z boson in pp collisions at $\sqrt{s}=7$ and 8 TeV with the ATLAS detector*, *Phys. Lett. B* **732** (2014) 8–27, [[1402.3051](#)].
- [33] CMS collaboration, S. Chatrchyan et al., *Search for a Higgs boson decaying into a Z and a photon in pp collisions at $\sqrt{s}=7$ and 8 TeV*, *Phys. Lett. B* **726** (2013) 587–609, [[1307.5515](#)].
- [34] CMS collaboration, V. Khachatryan et al., *Search for a Higgs boson decaying into $\gamma^*\gamma \rightarrow \ell\bar{\ell}\gamma$ with low dilepton mass in pp collisions at $\sqrt{s}=8$ TeV*, *Phys. Lett. B* **753** (2016) 341–362, [[1507.03031](#)].
- [35] C. Anastasiou, C. Duhr, F. Dulat, E. Furlan, T. Gehrmann, F. Herzog et al., *High precision determination of the gluon fusion Higgs boson cross-section at the LHC*, *JHEP* **05** (2016) 058, [[1602.00695](#)].
- [36] J. Alwall, R. Frederix, S. Frixione, V. Hirschi, F. Maltoni, O. Mattelaer et al., *The automated computation of tree-level and next-to-leading order differential cross sections, and their matching to parton shower simulations*, *JHEP* **07** (2014) 079, [[1405.0301](#)].
- [37] M. Grazzini, S. Kallweit, D. Rathlev and A. Torre, *$Z\gamma$ production at hadron colliders in NNLO QCD*, *Phys. Lett. B* **731** (2014) 204–207, [[1309.7000](#)].
- [38] J. M. Campbell, R. K. Ellis, Y. Li and C. Williams, *Predictions for diphoton production at the LHC through NNLO in QCD*, *JHEP* **07** (2016) 148, [[1603.02663](#)].
- [39] *Projections for measurements of Higgs boson cross sections, branching ratios and coupling parameters with the ATLAS detector at a HL-LHC*, Tech. Rep. ATL-PHYS-PUB-2013-014, CERN, Geneva, Oct, 2013.
- [40] CMS collaboration, *Projected Performance of an Upgraded CMS Detector at the LHC and HL-LHC: Contribution to the Snowmass Process*, in *Proceedings, Community Summer Study 2013: Snowmass on the Mississippi (CSS2013): Minneapolis, MN, USA, July 29-August 6, 2013*, 2013, [[1307.7135](#)].
- [41] G. T. Bodwin, F. Petriello, S. Stoynev and M. Velasco, *Higgs boson decays to quarkonia and the $H\bar{c}c$ coupling*, *Phys. Rev. D* **88** (2013) 053003, [[1306.5770](#)].
- [42] G. T. Bodwin, H. S. Chung, J.-H. Ee, J. Lee and F. Petriello, *Relativistic corrections to Higgs boson decays to quarkonia*, *Phys. Rev. D* **90** (2014) 113010, [[1407.6695](#)].
- [43] M. König and M. Neubert, *Exclusive Radiative Higgs Decays as Probes of Light-Quark Yukawa Couplings*, *JHEP* **08** (2015) 012, [[1505.03870](#)].

- [44] G. T. Bodwin, H. S. Chung, J.-H. Ee and J. Lee, *A new approach to the resummation of logarithms in Higgs-boson decays to a vector quarkonium plus a photon*, *Phys. Rev.* **D95** (2017) 054018, [[1603.06793](#)].
- [45] ATLAS collaboration, G. Aad et al., *Search for Higgs and Z Boson Decays to $J/\psi\gamma$ and $\Upsilon(nS)\gamma$ with the ATLAS Detector*, *Phys. Rev. Lett.* **114** (2015) 121801, [[1501.03276](#)].
- [46] G. Perez, Y. Soreq, E. Stamou and K. Tobioka, *Constraining the charm Yukawa and Higgs-quark coupling universality*, *Phys. Rev.* **D92** (2015) 033016, [[1503.00290](#)].
- [47] *Search for the Standard Model Higgs and Z Boson decays to $J/\psi\gamma$: HL-LHC projections*, Tech. Rep. ATL-PHYS-PUB-2015-043, CERN, Geneva, Sep, 2015.
- [48] G. F. Giudice and O. Lebedev, *Higgs-dependent Yukawa couplings*, *Phys. Lett.* **B665** (2008) 79–85, [[0804.1753](#)].
- [49] M. Bauer, M. Carena and K. Gemmler, *Flavor from the Electroweak Scale*, *JHEP* **11** (2015) 016, [[1506.01719](#)].
- [50] R. Harnik, J. Kopp and J. Zupan, *Flavor Violating Higgs Decays*, *JHEP* **03** (2013) 026, [[1209.1397](#)].
- [51] C. Delaunay, C. Grojean and G. Perez, *Modified Higgs Physics from Composite Light Flavours*, *JHEP* **09** (2013) 090, [[1303.5701](#)].
- [52] C. Delaunay, T. Flacke, J. Gonzalez-Fraile, S. J. Lee, G. Panico and G. Perez, *Light Non-degenerate Composite Partners at the LHC*, *JHEP* **02** (2014) 055, [[1311.2072](#)].
- [53] M. Blanke, G. F. Giudice, P. Paradisi, G. Perez and J. Zupan, *Flavoured Naturalness*, *JHEP* **06** (2013) 022, [[1302.7232](#)].
- [54] A. L. Kagan, G. Perez, T. Volansky and J. Zupan, *General Minimal Flavor Violation*, *Phys. Rev.* **D80** (2009) 076002, [[0903.1794](#)].
- [55] A. Dery, A. Efrati, G. Hiller, Y. Hochberg and Y. Nir, *Higgs couplings to fermions: 2HDM with MFV*, *JHEP* **08** (2013) 006, [[1304.6727](#)].
- [56] L. Da Rold, C. Delaunay, C. Grojean and G. Perez, *Up Asymmetries From Exhilarated Composite Flavor Structures*, *JHEP* **02** (2013) 149, [[1208.1499](#)].
- [57] A. Dery, A. Efrati, Y. Nir, Y. Soreq and V. Susić, *Model building for flavor changing Higgs couplings*, *Phys. Rev.* **D90** (2014) 115022, [[1408.1371](#)].
- [58] F. Bishara, J. Brod, P. Uttayarat and J. Zupan, *Nonstandard Yukawa Couplings and Higgs Portal Dark Matter*, *JHEP* **01** (2016) 010, [[1504.04022](#)].
- [59] C. Delaunay, T. Golling, G. Perez and Y. Soreq, *Enhanced Higgs boson coupling to charm pairs*, *Phys. Rev.* **D89** (2014) 033014, [[1310.7029](#)].
- [60] Y. Zhou, *Constraining the Higgs boson coupling to light quarks in the HZZ final states*, *Phys. Rev.* **D93** (2016) 013019, [[1505.06369](#)].
- [61] G. Perez, Y. Soreq, E. Stamou and K. Tobioka, *Prospects for measuring the Higgs boson coupling to light quarks*, *Phys. Rev.* **D93** (2016) 013001, [[1505.06689](#)].
- [62] I. Brivio, F. Goertz and G. Isidori, *Probing the Charm Quark Yukawa Coupling in Higgs+Charm Production*, *Phys. Rev. Lett.* **115** (2015) 211801, [[1507.02916](#)].
- [63] F. Bishara, U. Haisch, P. F. Monni and E. Re, *Constraining Light-Quark Yukawa Couplings from Higgs Distributions*, [1606.09253](#).

- [64] F. Yu, *Phenomenology of Enhanced Light Quark Yukawa Couplings and the $W^{\pm}h$ Charge Asymmetry*, *JHEP* **02** (2017) 083, [[1609.06592](#)].
- [65] L. M. Carpenter, T. Han, K. Hendricks, Z. Qian and N. Zhou, *Higgs Boson Decay to Light Jets at the LHC*, *Phys. Rev.* **D95** (2017) 053003, [[1611.05463](#)].
- [66] ATLAS collaboration, *b-jet tagging calibration on c-jets containing D^{*+} mesons*, .
- [67] ATLAS collaboration, T. A. collaboration, *Calibration of the performance of b-tagging for c and light-flavour jets in the 2012 ATLAS data*, .
- [68] *Performance and Calibration of the JetFitterCharm Algorithm for c-Jet Identification*, Tech. Rep. ATL-PHYS-PUB-2015-001, CERN, Geneva, Jan, 2015.
- [69] *Expected photon performance in the ATLAS experiment*, Tech. Rep. ATL-PHYS-PUB-2011-007, CERN, Geneva, Apr, 2011.
- [70] S. Catani, M. Fontannaz, J. P. Guillet and E. Pilon, *Cross-section of isolated prompt photons in hadron hadron collisions*, *JHEP* **05** (2002) 028, [[hep-ph/0204023](#)].